Controlling stimulated coherent spectroscopy and microscopy by a position-dependent phase

Chao-Yu Chung, Julie Hsu, Shaul Mukamel, and Eric O. Potma*
Department of Chemistry, University of California, Irvine Irvine, California 92697, USA
(Received 17 January 2013; published 26 March 2013)

We study the role of geometry-dependent phase shifts of the optical electric field in stimulated coherent spectroscopy, a special class of heterodyne optical spectroscopy techniques. We generalize the theoretical description of stimulated spectroscopy to include spatial phase effects, and study the measured material response for several representative excitation and detection configurations. Using stimulated Raman scattering microscopy as an example, we show that different components of the material response are measured by varying the position of the object in focus. We discuss the implications of the position-dependent phase in stimulated coherent microscopy and point out a detection configuration in which its effects are minimized.

DOI: 10.1103/PhysRevA.87.033833 PACS number(s): 42.65.Dr, 42.25.Hz

I. INTRODUCTION

Stimulated coherent optical techniques form a class of optical methods that include pump-probe techniques such as stimulated emission of electronic transitions, and Raman sensitive pump-probe techniques such as stimulated Raman loss and gain spectroscopy. These techniques are classified as stimulated because the signal is detected at a photon mode that is already occupied by photons of the excitation field. In a classical description, the signal can be viewed as an interference between an induced signal field and one of the excitation fields, at the point of the detector. Because the signal results from interferometric mixing of two fields, stimulated coherent techniques can be classified as a special form of heterodyne detection, where the excitation field acts as the local oscillator.

Unlike in regular heterodyne detection techniques, which involve a local oscillator with adjustable amplitude and phase, the phase difference between the interfering fields in stimulated optical techniques is not a freely adjustable parameter. Instead, it is determined by the material response and locked by the geometry of the excitation and detection. The latter aspect, the spatial configuration of the experiment, is usually not given due consideration in most theoretical descriptions of stimulated coherent optical techniques. This is not surprising, as for most spectroscopic measurements homogeneous samples and plane wave excitation can be assumed, in which the spatial phase of the configuration is fixed and may not be varied.

However, there are several experimental configurations in which the spatial phase of the fields is notably different from the familiar case of homogenous samples and plane wave excitation. For instance, in the limit of single molecule spectroscopy, the induced field can no longer be assumed uniform in the transverse plane, as it originates from a single point **r** in the sample. Consequently, the spatial phase characteristics of such an experiment are different compared to homogeneous samples, and the measured signal reflects different projections of the material response. Similarly, when tightly focused fields are used, the spatial phase needs to be taken into consideration explicitly in order to model the measured response correctly.

The issue of spatial phase is particularly relevant in nonlinear coherent microscopy, such as electronic pump-probe and stimulated Raman scattering (SRS) microscopy. The objects imaged in microscopy are often smaller than the wavelength of light, which implies that the spatial phase characteristics of homogeneous samples no longer apply. In addition, the spatial phase of the excitation fields, as exemplified by the Gouy phase shift, is a rapidly varying function on a micrometer scale. A proper description of stimulated signals in microscopy thus necessitates explicit consideration of the spatial phase.

Although spatial phase has received some attention in homodyne-detected coherent anti-Stokes Raman scattering (CARS) microscopy [1–5] and in angle-resolved four-wave mixing [6], so far it has not been studied in detail for stimulated coherent spectroscopy and microscopy. In this work, we provide a description of third-order stimulated signals that takes spatial phase explicitly into account. Using SRS as an example, we show that the measured material response is sensitive to the actual geometry of the experiment. We subsequently demonstrate theoretically and experimentally that, due to the presence of a spatially varying phase, spectral changes can be observed in the SRS spectrum as the position of a small object is varied in a focused beam geometry.

II. THEORY

In the classical description of stimulated coherent spectroscopy, the detected signal can be described in terms of classical wave interference in the far field. We first define the induced field E_s of frequency ω_s, which is generated at point **r** through a nonlinear process and detected at a far-field point **R**. At the detection point, the induced field is mixed with a local oscillator field E_{LO}, which is phase coherent with the former. The total intensity at the detector is then written as

$$S(\mathbf{R}) = \frac{n(\omega_s)c}{8\pi}|E_s(\mathbf{R}) + E_{\mathrm{LO}}(\mathbf{R})|^2 = I_s(\mathbf{R}) + I_{\mathrm{LO}}(\mathbf{R}) + 2\frac{n(\omega_s)c}{8\pi}\mathrm{Re}\{E_s(\mathbf{R}) \cdot E^*_{\mathrm{LO}}(\mathbf{R})\}, \quad (1)$$

where $n(\omega_s)$ is the refractive index of the material at frequency ω_s, c is the speed of light, and I_s, I_{LO} are the intensities of the induced signal and the local oscillator fields, respectively.

*epotma@uci.edu

Note that the fields $E(\mathbf{R})$ are complex with a given wave vector that depends parametrically on $\mathbf{R}$. We define the *heterodyne* contribution to the signal as

$$S_{\text{het}}(\mathbf{R}) = \frac{n(\omega_s)c}{4\pi}\text{Re}\{E_s(\mathbf{R}) \cdot E^*_{\text{LO}}(\mathbf{R})\}. \quad (2)$$

Stimulated coherent optical signals can generally be understood in terms of Eq. (2) when one of the excitation fields provides the local oscillator, i.e., the induced field interferes with one of the driving fields. In the following, we shall discuss the role of spatial phase in stimulated coherent spectroscopy by using a Raman sensitive pump-probe experiment as an example. However, the results discussed here hold more generally for other stimulated coherent spectroscopy techniques as well.

In the Raman-sensitive pump probe, two incoming fields ω_1 and ω_2, where $\omega_1 > \omega_2$, induce a third-order polarization in the material. Raman resonances occur when $\omega_1 - \omega_2$ is close to a (vibrational) resonance in the material, which gives rise to stimulated Raman contributions at the detection frequencies ω_1 and ω_2. The signal detected at ω_1 is commonly called the stimulated Raman loss (SRL) signal. We will focus on this signal for the remainder of this work. The nonlinear polarization component responsible for the SRL signal is

$$P^{(3)}(\omega_1,\mathbf{r}) = \chi^{(3)}(\omega_1,\mathbf{r})|E_2(\mathbf{r})|^2 E_1(\mathbf{r}), \quad (3)$$

where $\chi^{(3)}(\omega_1,\mathbf{r})$ is the third-order nonlinear susceptibility, which describes the efficiency of the third-order material response at frequency ω_1 and at point $\mathbf{r}$ in the sample. The time harmonic electric field $\tilde{E}$ measured in the far field is a real quantity that can be related to the field at position $\mathbf{r}$ as follows:

$$\tilde{E}(\mathbf{R},t) = E(\mathbf{r})e^{-i(\omega t+\Phi)} + \text{c.c.} \quad (4)$$

Here we have allowed for a spatial phase shift Φ of the field at point $\mathbf{R}$ relative to the phase at the excitation point $\mathbf{r}$. The value of the phase shift depends on the excitation and detection geometry, and several representative cases are discussed below. Using this notation, and assuming no significant depletion of the driving field, the spatial parts of the induced field and the local oscillator field can be written as

$$E_s(\mathbf{R}) \propto P^{(3)}(\omega_1,\mathbf{r})e^{-i\phi}, \quad (5)$$

$$E_{\text{LO}}(\mathbf{R}) = E_1(\mathbf{R}) \approx E_1(\mathbf{r})e^{-i\alpha}, \quad (6)$$

where ϕ is the spatial phase of the *induced field* at $\mathbf{R}$ relative to the phase at $\mathbf{r}$, and α measures a similar spatial phase shift between $\mathbf{r}$ and $\mathbf{R}$ for the *excitation field*.

Next, we discuss the form of the signal in three relevant configurations of the SRL experiment, with fixed values for ϕ and α, followed by a discussion of an experimental configuration where α is an adjustable control parameter.

A. Plane wave excitation of a sheet of dipoles

For plane wave excitation, the excitation fields have a uniform phase in the transverse plane. We can model a thin sample that is invariant in the lateral dimension as an infinite sheet of point dipoles, oriented perpendicular to the propagation direction of the fields, and located at z as in Fig. 1(a). Using plane wave excitation, the induced field

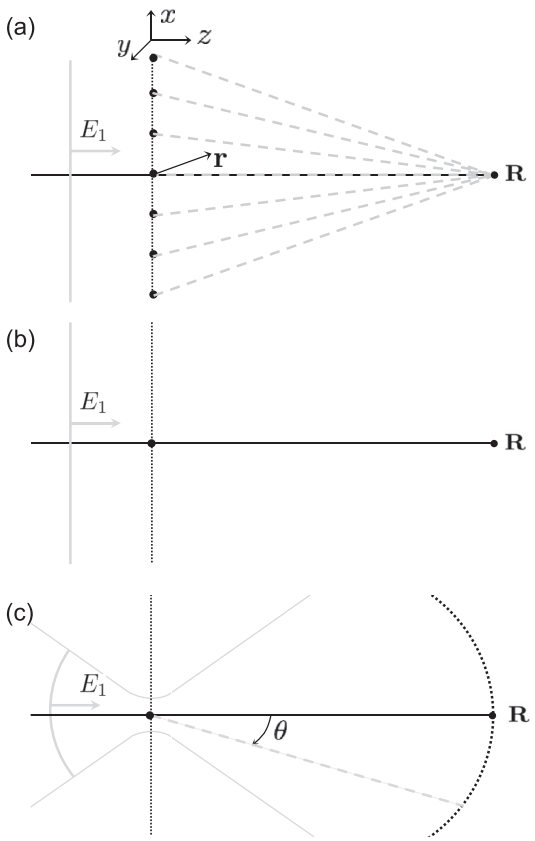

FIG. 1. Detection geometries in stimulated Raman scattering spectroscopy. In each case, excitation is in the vicinity of $\mathbf{r}$ and detection is at the far-field point $\mathbf{R}$. (a) Plane wave excitation of a sheet of point dipoles (black dots), uniformly positioned in the transverse plane. Dashed lines indicate the propagation path of each dipole emitter to the far-field point $\mathbf{R}$. (b) Plane wave excitation of a single dipole emitter. (c) Focused excitation of a dipole emitter. Angle θ defines the angle between the optical axis and the propagation path of a ray toward the far-field hemispherical surface. Note that maximum value of θ, as seen by the far-field detector, relates to the numerical aperture of the detection system.

radiated from the collective dipoles at z and detected at the far-field point $\mathbf{R}$ is proportional to the induced polarization at $\mathbf{r}$, but shifted by a spatial phase factor $-\frac{1}{2}\pi$ [7,8]. In the plane wave approximation, using $\phi = -\frac{1}{2}\pi$, the following relation is obtained from Eq. (5):

$$E_s(\mathbf{R}) \propto i\,P^{(3)}(\mathbf{r}). \quad (7)$$

In this formulation, the phase relation between E_s and $P^{(3)}$ in this expression is equivalent to the phase relation obtained by the plane wave solution of the nonlinear wave equation [9,10]. Using Eqs. (2) and (7), the general expression for the heterodyne contribution to the signal in the plane wave approximation can be found as [10]

$$S_{\text{het}}(\mathbf{R}) \propto -\text{Im}\{\text{P}^{(3)}(\mathbf{r})\text{E}^*_{\text{LO}}(\mathbf{R})\}. \quad (8)$$

For the SRL process, using Eq. (3), the signal is recast as follows:

$$S_{\text{SRL}}(\mathbf{R}) \propto -\text{Im}\{\chi^{(3)}(\omega_1,\mathbf{r})|\text{E}_2(\mathbf{r})|^2\text{E}_1(\mathbf{r})\text{E}^*_1(\mathbf{R})\}. \quad (9)$$

This relation contains the term $E_1(\mathbf{r})E_1^*(\mathbf{R})$, which carries phase information that depends solely on the spatial profile of the excitation field. Using Eq. (6), this latter term can be rewritten as $|E_1(\mathbf{r})|^2 e^{i\alpha}$. For plane waves, the spatial phase of the excitation field along the propagation direction is invariant, i.e., $\alpha = 0$. We can thus write

$$S_{\mathrm{SRL}}(\mathbf{R}) \propto -|E_2(\mathbf{r})|^2|E_1(\mathbf{r})|^2\mathrm{Im}\{\chi^{(3)}(\omega_1,\mathbf{r})\}. \quad (10)$$

Equation (10) is a familiar result: It shows that the SRL signal is proportional to the imaginary part of the third-order material response and proportional to the product of the excitation intensities I_1 and I_2, at the excitation location $\mathbf{r}$ only. The current analysis points out that this result originates from the fact that, for the plane wave geometry, $\phi = -\frac{1}{2}\pi$ for the induced field and the spatial phase of E_1 at the point of excitation and detection is invariant. However, different results can be expected when the value of ϕ is different or the spatial phase of E_1 is no longer spatially invariant.

B. Plane wave excitation of a single dipole

When the sheet of dipoles is replaced by a single dipole, the induced field exhibits a phase that is spatially invariant, i.e., $\phi = 0$. This situation is sketched in Fig. 1(b). We can now write

$$E_s(\mathbf{R}) \propto P^{(3)}(\mathbf{r}). \quad (11)$$

Noting that, as before, the spatial phase of E_1 at $\mathbf{r}$ and $\mathbf{R}$ is identical, i.e., $\alpha = 0$, the SRL signal is written as

$$S_{\mathrm{SRL}}(\mathbf{R}) \propto |E_2(\mathbf{r})|^2|E_1(\mathbf{r})|^2\mathrm{Re}\{\chi^{(3)}(\omega_1,\mathbf{r})\}. \quad (12)$$

Comparing Eqs. (10) and (12), it can be seen that different aspects of the material response are measured when the geometry of the experiment is altered. By replacing the sheet of dipoles with a single dipole, the spatial phase characteristics of the problem have changed, and the experiment is now sensitive to the real part of the nonlinear susceptibility.

C. Single dipole in the focal plane

We next consider a single dipole placed in the focal plane of focused excitation fields, as shown in Fig. 1(c). In this limit, $\phi = 0$, and the SRL signal is found as

$$S_{\mathrm{SRL}}(\mathbf{R}) \propto \mathrm{Re}\{\chi^{(3)}(\omega_1,\mathbf{r})|E_2(\mathbf{r})|^2 E_1(\mathbf{r})E_1^*(\mathbf{R})\}. \quad (13)$$

Unlike the case of plane wave excitation, the spatial phase of E_1 at the point of excitation and detection is no longer the same. The Gouy phase shift imparts a spatial phase shift of magnitude $\frac{1}{2}\pi$ between the focal plane at $\mathbf{r}$ and a far-field point $\mathbf{R}$ in the excitation field [11–13]. Using $\alpha = \frac{1}{2}\pi$ in Eq. (13), we find that the measured SRL signal is described by an expression similar to Eq. (10): The SRL signal in this focused configuration is proportional to the imaginary part of the third-order susceptibility. This configuration is most relevant to SRL microscopy. Hence, when small objects are present in the focal plane, the SRL imaging contrast is determined by $S \propto -\mathrm{Im}\{\chi^{(3)}(\omega_1)\}$.

D. Single dipole in the focal volume

In the examples considered above, the spatial phase shift of the excitation field and induced field assumed fixed values. As a consequence, the SRL experiment was sensitive to either the real or imaginary part of the nonlinear susceptibility. The focused field geometry, however, allows for an adjustable phase shift between the excitation and the induced field. We now consider a single dipole positioned in a focused excitation field. Recall that, for a single dipole, the spatial phase of the induced field is invariable ($\phi = 0$). The variation of the spatial phase is fully contained in the excitation field. An adjustable phase shift can be achieved by positioning the dipole at different locations along the optical axis z. The excitation field undergoes a Gouy phase shift of total magnitude π along this coordinate, and α is now a position-dependent phase shift $\alpha(\mathbf{r})$ with a value in the interval $[0,\pi]$.

The SRL signal can then be written as

$$S_{\mathrm{SRL}}(\mathbf{R}) \propto I_1(\mathbf{r})I_2(\mathbf{r})[\mathrm{Re}\{\chi^{(3)}(\omega_1,\mathbf{r})\}\cos\alpha(\mathbf{r}) - \mathrm{Im}\{\chi^{(3)}(\omega_1,\mathbf{r})\}\sin\alpha(\mathbf{r})], \quad (14)$$

where I_1 and I_2 are the intensities of the excitation fields at ω_1 and ω_2, respectively. Equation (14) explicitly shows that the measured signal in the far field depends on the position-dependent phase $\alpha(\mathbf{r})$, i.e., different components of the material response are measured depending on position of the dipole in the focused excitation field, as sketched in Fig. 2. As before, when the dipole particle is placed exactly in the focal plane, then $\alpha(z = 0) = \frac{1}{2}\pi$ and the SRL signal is $S \propto -\mathrm{Im}\{\chi^{(3)}(\omega_1)\}$. However, when the particle is placed above or below the focal plane, $\alpha \neq \frac{1}{2}\pi$ and the SRL

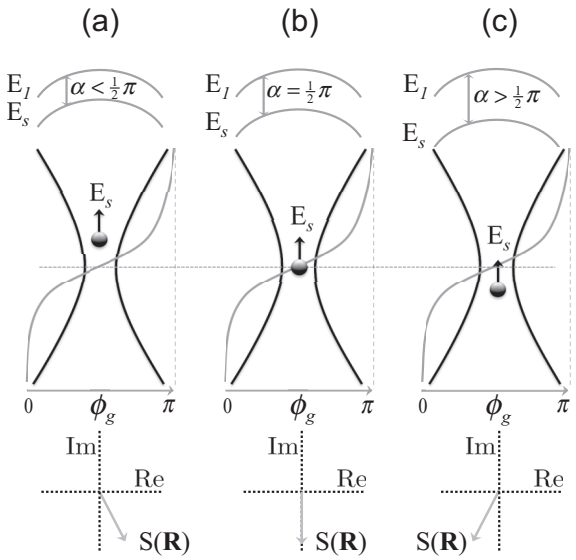

FIG. 2. Principle of position-dependent phase shift. The Gouy phase shift ϕ_g is sketched as a gray line. The phase shift α of the excitation field is variable due to the position-dependent ϕ_g, and introduces a position-dependent phase shift between E_s and E_1 in the far field. (a) Object is above the focal plane, resulting in $\alpha < \frac{1}{2}\pi$. (b) Object is at the focal plane, and $\alpha = \frac{1}{2}\pi$. (c) Object is below the focal plane, giving rise to $\alpha > \frac{1}{2}\pi$. The insets schematically show the heterodyne signal $S(\mathbf{R})$ in the complex plane for each situation.

signal contains contributions of $\mathrm{Re}\{\chi^{(3)}(\omega_1)\}$. The measured spectral profile critically depends on the relative contributions of the real and imaginary components to the nonlinear susceptibility. We examine the extent of these spectral changes both computationally and experimentally in Sec. IV.

III. MATERIALS AND METHODS

The SRL experiments in this work were performed on a regular coherent Raman scattering microscope. The excitation beams at λ_1 and λ_2 were derived from an optical parametric oscillator (OPO, Levante Emerald) pumped by a 532-nm, 7-ps, 76-MHz mode-locked Nd:vanadate laser (Picotrain, High-Q). The excitation beam at λ_2 was fixed at 1064 nm, whereas the excitation beam at λ_1 was tuned within the 795–811-nm range. The pump and Stokes beams were overlapped both spatially and temporally on a dichroic beam combiner, and sent into a laser scanner (Fluoview 300, Olympus), illuminating the specimen with a 60×, 1.2-NA, water-immersion objective lens (UPlanSApo Olympus) mounted on an inverted microscope (IX71, Olympus). To monitor stimulated Raman loss, the λ_2 beam was modulated at 10 MHz with an acoustic optical modulator (Crystal Technology). The modulated pump intensity was collected by a 0.9-NA condenser and detected by a photodiode (FDS1010, Thorlabs), and the signal was demodulated with a home-built lock-in amplifier. To achieve rapid hyperspectral SRL imaging with spectral resolution of 5 cm^{-1}, several parameters of the OPO, including crystal temperature, Lyot filter, and cavity length, were automatically tuned with home-written software.

To compensate for drift in the distance between the objective lens and the sample, we have incorporated a z-axis stabilizer based on an interferometer design. The light source of the interferometer was a 635-nm diode laser, which produces a position-dependent interferogram onto a CCD camera. The phase of this interferogram was retrieved for determining the z drift, and a z-axis controller (MFC-2000, Applied Scientific Instrumentation) was used to compensate for the distance variations with a resolution of 0.1 μm.

We used 0.47 μm polystyrene beads (Polysciences) as our target for the SRL experiments. The beads were first mixed with agarose gel, and subsequently deposited onto a glass coverslip. After drying of the mixture, water was added to the sample and the sample was sealed with a second coverslip.

The computations in this study were based on vectorial focal field calculations. Details can be found in previous work [14]. Briefly, the nonlinear polarization resulting from a driven dipole, placed in the focal volume, was approximated as a voxel with a volume of $50 \times 50 \times 100$ nm^3 in which the polarization was uniform and given by Eq. (3). The focal fields of the incident laser beams were calculated from diffraction theory [15]. The far-field radiation from the dipole measured at point $\mathbf{R}$ was added to the incident field at the same location, and the detected signal was calculation according to Eq. (2). For the calculations, $\lambda_2 = 1064$ nm, and λ_1 was varied in the wavelength range relevant to the range examined in the experiments. The polarization of the input fields was directed along the x axis. The numerical aperture of the excitation objective used in the calculations was 1.2W, where W implies that the immersion medium is water. The vibrational resonance of $\chi^{(3)}$ was approximated as a single Lorentzian line with a 5-cm^{-1} linewidth.

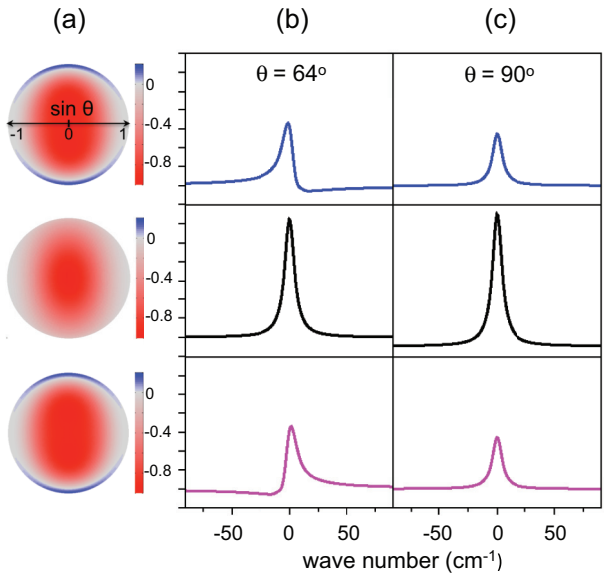

FIG. 3. (Color online) Calculation of the far-field SRL signal for different positions of the object. (a) Normalized far-field interference pattern when the object is 0.5 μm above the focal plane (top), at the focal plane (middle), and 0.5 μm below the focal plane (bottom). Red indicates negative (loss) and blue indicates positive (gain). (b) SRL spectra for a detection NA of 0.9 (64°) calculated for the different positions of the object. Note that the SRL spectra are plotted here as positive to facilitate the bandshape interpretation. (c) SRL spectra for a full detection aperture (90°). Excitation NA = 1.2W

IV. RESULTS AND DISCUSSION

We first investigated the SRL signal computationally as a function of the axial position of a subwavelength particle in focus. The first column in Fig. 3 compares the interference pattern of the on-resonance SRL signal, as seen on the far-field hemispherical surface, slightly above the focal plane, at the focal plane, and slightly below the focal plane. On the optical axis ($\theta = 0$), a negative signal is observed for all particle positions. This corresponds to an expected loss signal. However, for particles above or below the focal plane, we see that at some larger θ the measured signal becomes positive, corresponding to the blue areas in the radiation profile. This demonstrates that the interference between the induced field and the incident field is not spatially uniform. Note that the radiation profile is not rotationally symmetric because of the linear input polarization of the field.

Importantly, it can be seen that the interference pattern is dependent on the axial position of the particle. This results from the spatially dependent phase α, which, according to Eq. (14) alters the signal as the particle position is changed. The second column in Fig. 3 highlights this point, which depicts calculations of the SRL signal with a collection numerical aperture of 0.9 in air. When the particle is positioned at the focal plane ($\alpha = \frac{1}{2}\pi$), the spectrum is proportional to $\mathrm{Im}\{\chi^{(3)}\}$.

When the particle is found above or below the focal plane ($\alpha \neq \frac{1}{2}\pi$), portions of Re$\{\chi^{(3)}\}$ contribute to the signal, resulting in a dispersive lineshape.

The dispersive lineshapes imply that the measured SRL signal is not purely a loss signal. At some frequencies, the SRL signal is a gain signal. At first sight, this picture seems in conflict with the quantum description of the SRL process. In the quantum description, a ω_1 photon is absorbed (loss), which, in combination with an emitted ω_2 photon, leaves the molecule in the vibrationally excited state. An emission of a ω_1 photon (gain) would imply that the molecule is initially in the vibrationally excited state instead of in the ground state, which is physically not the case. This apparent ambiguity is solved when integrating the far-field radiation within the solid angle of the entire hemisphere, instead of just within the detection aperture. The full aperture spectral signal is plotted in the third column of Fig. 3. The SRL signal is now a loss signal for all positions of the molecule, represented by a undistorted Lorentzian lineshape. Hence, there is no conflict between the classical interference picture and the quantum description.

We next studied the effect of spatial phase on the SRL signal experimentally. In Fig. 4, experimental SRL spectra are shown for 0.47-μm polystyrene beads in the region of the vinyl stretching vibration. It can be seen that the SRL spectrum changes when the position of the particle is changed along the optical axis. When the particle is below the focal plane, a depression on the low energy side is seen. In addition, above the focal plane, the spectral density on the low energy side increases, analogous to the trends presented in Fig. 3.

To verify the position-dependent spectral features, we determined the real and imaginary parts of the polystyrene response with the help of a Kramers-Kronig transformation of the Raman spectrum. Using Eq. (14), we calculated the expected SRL spectra for different values of $\alpha(\mathbf{r})$. It can be seen that the experimental spectra at $z = -1.0$ μm and $z = 1.0$ μm are well reproduced for an effective spatial phase of $\alpha_{\text{eff}}(\mathbf{r}) \approx \frac{1}{2}\pi + 20^\circ$ and $\alpha_{\text{eff}}(\mathbf{r}) \approx \frac{1}{2}\pi - 20^\circ$, respectively. This calculation confirms that subwavelength particles can sense the spatial phase gradient of the excitation field, which translates into an effective phase shift that deviates from $\frac{1}{2}\pi$ when the particle is moved away from the focal plane.

Note that the physics that underlies the dispersive SRL lineshapes is similar in nature to the origin of the lineshapes observed in single molecule absorption microscopy [16–18]. Our work extends previous observations for electronic absorptions to the regime of vibrational absorptions as seen in a stimulated Raman process.

In CARS microscopy, spatial phase effects between a small particle and the nonresonant background of the bulk have recently been pointed out [4]. In SRS microscopy, the electronic nonresonant background is intrinsically suppressed, and interference effects between the nonresonant and resonant field components are absent. Because the dispersion-related wave-vector mismatch is zero in SRS, the technique is often interpreted as being completely free of spatial phase effects. Nonetheless, as shown in this work, spatial phase effects do play a role in SRS microscopy. The experiments shown in Fig. 4 underline that differences in the SRS spectral profile

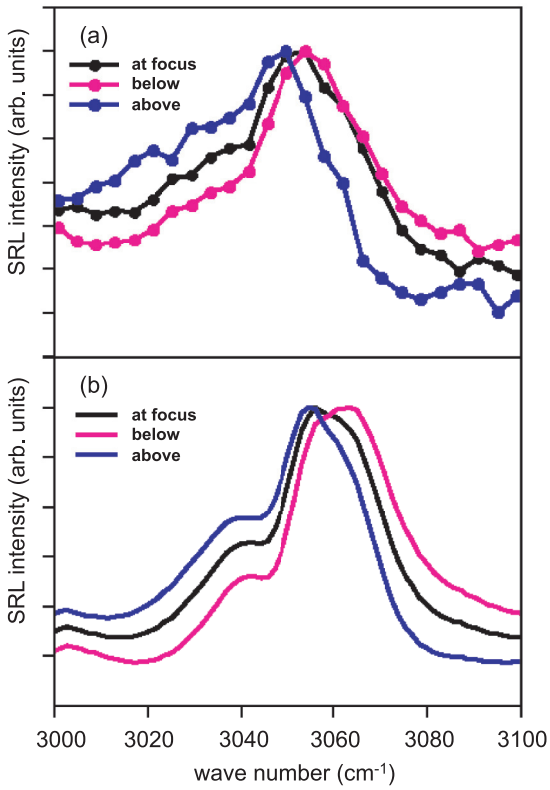

FIG. 4. (Color online) SRL spectra of a 0.47-μm polystyrene bead in the vinyl stretching range as a function of focal position. (a) Experimental SRL spectra for particle position $z = -1.0$ μm (magenta; bottom curve at 3000 wave-numbers), $z = 0$ μm (black; middle curve), and $z = 1.0$ μm (blue; top curve). (b) Calculation of SRL spectra, based on Eq. (14), for a phase shift $\alpha = 70^\circ$ (magenta; bottom curve at 3000 wave-numbers), $\alpha = 90^\circ$ (black; middle curve), and $\alpha = 110^\circ$ (blue; top curve). Excitation NA = 1.2W, detection NA = 0.9, and $\lambda_2 = 1064$ nm.

can be expected for individual particles as a function of their position in the focal volume. These effects are expected to be strongest for particles much smaller than the wavelength of light, such that they can be interpreted as single dipole emitters. Importantly, our work demonstrates that position-dependent spectral changes, though small, can be observed even for finite-sized particles that approach the wavelength of light.

Although in practice the reported effects are of minor importance to routine biological imaging, this work emphasizes that a detailed spectroscopic interpretation of SRS spectra acquired in the microscope should include spatial phase effects. Spectra can be interpreted with the help of Eq. (14) and an effective spatial phase α_{eff}. Our study also shows that spatial phase artifacts are largest when the signal is collected over a relatively small cone angle. Larger collection angles reduce the effects of spatial phase. Full suppression of these effects can be achieved when the signal is collected over the full hemisphere. In this regard, the favored detection geometry, the highest possible detection NA, is similar to the one employed to suppress other nonlinear imaging artifacts such as thermal lensing [5]. Our work thus underlines that the

use of high detection NAs is strongly recommended in SRS microspectroscopy of subwavelength particles.

V. CONCLUSION

In this work, we studied the effect of spatial phase, which can differ among excitation and detection geometries, in stimulated coherent spectroscopy. We found that the measured material response can vary notably depending on the spatial properties of the excitation field, the size of the object, and the detection configuration. We identified two relevant parameters: ϕ, which is the spatial phase shift of the induced field between the point of excitation and detection, and α, which measures the phase shift of the excitation field. Using these parameters, we retrieved the signal for the case of SRS in the plane wave limit, both for homogeneous samples and for point dipoles. In the particular case of SRS microscopy, we demonstrated theoretically and experimentally that the spectra of small particles are affected by a position-dependent phase shift. These microspectroscopy artifacts can be suppressed by increasing the NA of the detection.

ACKNOWLEDGMENTS

This work was supported by the National Science Foundation, Grants No. CHE-0847097 and No. CHE-0802913 to E.O.P.. S.M. gratefully acknowledges support from the National Institutes of Health, Grant No. GM-59230, and the National Science Foundation, Grant No. CHE-1058791. We are grateful to Yong Wang for his help with the sample position stabilization. We thank Professor Sunney Xie, Harvard University, for useful discussions that formed the motivation for this work.

[1] J. X. Cheng, A. Volkmer, and X. S. Xie, J. Opt. Soc. Am. B **19**, 1363 (2002).
[2] V. V. Krishnamachari and E. O. Potma, J. Opt. Soc. Am. A **24**, 1138 (2007).
[3] D. Gachet, S. Brustlein, and H. Rigneault, Phys. Rev. Lett. **104**, 213905 (2010).
[4] I. Popov, A. F. Pegoraro, A. Stolow, and L. Ramunno, Opt. Express **19**, 5902 (2011).
[5] I. Popov, A. F. Pegoraro, A. Stolow, and L. Ramunno, Opt. Lett. **37**, 473 (2012).
[6] I. P. Mercer, Phys. Rev. A **82**, 043406 (2010).
[7] R. Feynman, *The Feynman Lectures on Physics*, Vol. I, Sec 30-7 (Addison Wesley, Reading, 1964).
[8] M. Sargent III, M. O. Scully, and W. E. Lamb, *Laser Physics*, Appendix A (Addison-Wesley, Reading, 1974).
[9] R. Boyd, *Nonlinear Optics* (Academic Press, San Diego, 2003).
[10] S. Mukamel, *Principles of Nonlinear Optical Microscopy* (Oxford University Press, New York, 1995).
[11] L. G. Gouy, C. R. Acad. Sci. Paris **110**, 1251 (1890).
[12] S. Feng and H. G. Winful, Opt. Lett. **26**, 485 (2001).
[13] R. W. Boyd, J. Opt. Soc. Am. **70**, 877 (2001).
[14] V. Raghunathan and E. O. Potma, J. Opt. Soc. Am. A **27**, 2365 (2010).
[15] B. Richards and E. Wolf, Proc. R. Soc. London A **253**, 358 (1959).
[16] I. Gerhardt, G. Wrigge, M. Agio, P. Bushev, G. Zumofen, and V. Sandoghdar, Opt. Lett. **32**, 1420 (2007).
[17] I. Gerhardt, G. Wrigge, P. Bushev, G. Zumofen, M. Agio, R. Pfab, and V. Sandoghdar, Phys. Rev. Lett. **98**, 033601 (2007).
[18] M. Pototschnig, Y. Chassagneux, J. Hwang, G. Zumofen, A. Renn, and V. Sandoghdar, Phys. Rev. Lett. **107**, 063001 (2011).